

METHODOLOGICAL NOTES PACS numbers: 02.30.Em, 95.10.Ce, 96.15.De, 96.30.Wr, **97.82.–j**

From Kepler's ellipses — to R-toroids

B.P. Kondratyev

DOI: https://doi.org/10.3367/UFNe.2025.09.040024

Contents

1. Introduction **392**
2. Inverse square law and the two-body problem are the basis of celestial mechanics **393**
3. Lagrange osculating ellipses and perturbation theory **393**
4. Laplace integral of motion and its applications **393**
4.1 Two methods of setting problems for two-planet problems of extrasolar systems; 4.2 Orbital orientation vectors; 4.3 Secular evolution equations for orbit orientation vectors; 4.4 Solving evolution equations; 4.5 Application of the new method 2 to the two-planet exosystem HD 206893
5. Gaussian ring and its potential **395**
5.1 Gaussian ring potential; 5.2 Systems of two Gaussian rings. The mutual gravitational energy of these rings
6. Problem of confinement of rings around small bodies in the Solar system **398**
6.1 Nonplanetary type rings around small bodies; 6.2 Evolution equations for two rings in collective variables in the central field; 6.3 Ring stabilization conditions; 6.4 Restriction on Haumea ring mass
7. Two-dimensional generalization of the precessing Gaussian ring (R-disk model) **399**
7.1 The R-ring structure; 7.2 R-ring potential; 7.3 Applying the R-ring model
8. Three-dimensional generalization of the precessing Gaussian ring (R-toroid Model) **401**
8.1 Geometry of the R-toroid figure; 8.2 Density and potential distribution in R-toroid; 8.3 Mutual energy of the R-toroid and the outer Gaussian ring. Equations of secular evolution of osculating orbits of bodies
9. Application of the R-toroid model **403**
9.1 Some limitations on the application of the R-toroid model; 9.2 The two-planet problem (star + two planets); 9.3 The ratio of nodal and apsidal precession periods; 9.4 Secular evolution of exoplanetary systems. The three R-toroid method
10. Conclusion **404**
References **405**

Abstract. **An overview of new directions in modern celestial mechanics is given. The starting point is the Gaussian ring, the gravitational potential of which is obtained in analytical form. Instead of osculating Keplerian elements, a set of new variables is introduced: these are the Laplace and Hamilton vectors, as well as the vector of the orbital angular momentum of the body. In the linear approximation, the evolution equations in new variables are obtained, replacing the classical Lagrange equations. The method is tested on the exosystem HD 206893. The problem of confinement of rings around small celestial bodies is considered. Two new approaches based on two-dimensional (R-disk) and three-dimensional (R-toroid) generalizations of precessing Gauss rings are presented. The methods are tested by solving problems on the dynamics of stellar rings in the Galaxy and the secular evolution of orbits in various exoplanet systems.**

B.P. Kondratyev
(1) Lomonosov Moscow State University,
Shternberg State Astronomical Institute,
Universitetskii prosp. 13, 119234 Moscow, Russian Federation
(2) Central Astronomical Observatort Russian Academy of Sciences
at Pulkovo, Pulkovskoe shosse 65/1, 196140 St. Petersburg,
Russian Federation
E-mail: work@boris-kondratyev.ru

Received 17 August 2025
Uspekhi Fizicheskikh Nauk **196** (4) 422 – 435 (2026)
Translated by the authors

Keywords: Kepler ellipses, Gaussian ring and its potential, orbital orientation vectors, confinement of rings around small celestial bodies, precession of Gauss rings: R-ring and R-toroid models, dwarf planet Haumea, two-planet problems, circumbinary exosystems

1. Introduction

The science of planetary motion has traveled a difficult path from the astrological manipulations of the priests to the inventive kinematic method of the epicycles of ancient astronomers. Hipparchus, Eudoxus and Ptolemy developed the theory of epicycles, discovered the precession of the Earth's rotation axis and the change in the longitude angle in the motion of the Moon. Let's note the fact connecting the two epochs: it turns out that the point of Ptolemy's equant (from which the planet's motion seems uniform) is nothing more than the point of the second (empty) focus of the Keplerian ellipse.

The theory of circular epicycles remained the core of astronomical knowledge for over twenty centuries. But Kepler's three laws completely changed the picture of planetary motion. Complex theoretical models based on combinations of uniform circular motions were replaced by the simple and physically clear kinematics of planetary motion in ellipses with the Sun at one focus. And although the revolution in astronomy wrought by Copernicus and his followers (Bruno, Kepler, Galileo) did not yet extend beyond the kinematic approach, the foundation had been laid: Kepler's ellipses remain a test of one's *Homo Sapiens* status today!

With the advent of the general dynamical method in the works of Newton and Euler, the art of creating models based on differential equations of motion arose and began to improve in celestial mechanics. *Gradually, a special field of thought was formed in celestial mechanics, outside of which any discovery cannot be made or properly understood.*

Returning to the main topic, we emphasize that celestial mechanics (in a broader sense, 'dynamic astronomy') studies almost everything that moves and rotates in space: from dust particles to comets and asteroids, from artificial satellites of the Earth, from planets and their satellites to stars and galaxies. The development of celestial mechanics [1–5] it went through a rich practice of various applications, and the range of tasks in it is exceptionally wide. The discovery of exoplanetary systems around other stars has been a significant stimulus for the development of astronomy. This significantly expanded the range of new tasks and allowed for a new approach to many problems of dynamic astronomy.

2. Inverse square law and the two-body problem are the basis of celestial mechanics

The motion of two bodies in this problem is described by a system of sixth-order differential equations [3]

$$\ddot{\mathbf{r}} + \kappa^2 \frac{\mathbf{r}}{r^3} = 0\,, \quad \kappa^2 = G(M+m)\,. \tag{2.1}$$

There are five independent first integrals of motion in this problem:

$$\mathbf{V}^2 = \dot{\mathbf{r}}^2 = \frac{2\kappa^2}{r} + h \quad \text{energy integral}\,, \tag{2.2}$$

$$\mathbf{C} = [\mathbf{r} \times \mathbf{V}] \quad \text{vector area integral}\,, \tag{2.3}$$

$$\mathbf{L} = [\mathbf{V} \times \mathbf{C}] - \kappa^2 \frac{\mathbf{r}}{r} \quad \text{Laplace vector integral} \quad (+\text{Runge}-\text{Lenz})\,, \tag{2.4}$$

There are two additional relationships

$$[\mathbf{L} \times \mathbf{C}] = 0\,, \quad \mathbf{L}^2 = \kappa^4 + h\mathbf{C}^2\,. \tag{2.5}$$

Mathematically, the two-body problem has been solved, but in its astronomical aspect, ample scope for creativity remains. The two-body problem [2, 3] is not only an unchanging beacon in a boundless sea of disturbed motion; it also represents a vast complex of problems in dynamical astronomy: here you can trace the chains of ideas from Kepler orbits to osculating Lagrange ellipses, from Gaussian rings — up to models based on precessing analogues of these rings.

3. Lagrange osculating ellipses and perturbation theory

By the beginning of the 19th century, the baton had passed from Kepler's ellipses to osculating Lagrange ellipses, and on their basis, through the efforts of many scientists (Laplace, Delaunay, Encke, Hansen, Hill, Cowell), perturbation theory appeared [2, 3, 6]. Using Lagrange's five equations for osculating ellipses [2, 3] (a — semi-major axis, e — eccentricity, i — inclination, ω — argument of periapsis, Ω — longitude of ascending node, R — disturbance function)

$$\frac{\mathrm{d}a}{\mathrm{d}t} = \frac{2}{n_0 a}\frac{\partial R}{\partial M_0}\,, \quad \frac{\mathrm{d}e}{\mathrm{d}t} = \frac{1-e^2}{e n_0 a^2}\frac{\partial R}{\partial M_0} - \frac{\sqrt{1-e^2}}{e n_0 a^2}\frac{\partial R}{\partial \omega}\,,$$

$$\frac{\mathrm{d}i}{\mathrm{d}t} = \frac{\cos i}{n_0 a^2 \sqrt{1-e^2}\sin(i)}\frac{\partial R}{\partial \omega} - \frac{1}{n_0 a^2\sqrt{1-e^2}\sin i}\frac{\partial R}{\partial \Omega}\,,$$

$$\frac{\mathrm{d}\omega}{\mathrm{d}t} = \frac{\sqrt{1-e^2}}{e n_0 a^2}\frac{\partial R}{\partial e} - \cos i \frac{\partial \Omega}{\mathrm{d}t}\,,$$

$$\frac{\mathrm{d}\Omega}{\mathrm{d}t} = \frac{1}{n_0 a^2\sqrt{1-e^2}\sin i}\frac{\partial R}{\partial i} \tag{3.1}$$

it has become possible to find answers to the most difficult questions of celestial mechanics when Kepler's laws are only approximately fulfilled. Essentially, perturbation theory is the idea that one can study something unknown starting from a known quantity. One of its main methods is to take an ellipse as an initial (intermediate or reference) orbit, and then decompose the deviations between the actual and reference orbits into a series. However, these series don't always work (due to the presence of terms with small denominators). In this situation, Hansen cleverly proposed the idea of using a more complex curve, rather than an ellipse, as the reference orbit. Then, the series for the deviations of the actual orbit from the adopted reference orbit won't contain inconvenient terms.

Perturbation theory now makes extensive use of methods based on averaging orbits over 'fast' variables. Our review examines various variants of averaging methods.

4. Laplace integral of motion and its applications

First of all, the modulus of the vector integral (2.4) is equal (up to κ^2) to the eccentricity of the Kepler ellipse [7]

$$L = \kappa^2 e\,. \tag{4.1}$$

The Laplace vector $\mathbf{L}$ is directed toward the orbit's pericenter. Similarly, an auxiliary Hamilton vector $\mathbf{H}$ is introduced, directed along the minor axis of the ellipse and having the same modulus $H = \kappa^2 e$.

But the Laplace vector is the integral of motion only for a force inversely proportional to the square of the distances. In practice, however, there are always additional forces (perturbations). If the perturbing force is also central, the Laplace vector slowly rotates, and apsidal precession of the orbit occurs. Example: the effect of general relativity — perturbation in accordance with the inverse cube law leads to precession of the orbit of Mercury $43''$ for one hundred years [8].

But in most cases (for example, in the two-planet problem) the perturbation forces of the planets in orbits are not central, and then the dynamics of the Laplace vector becomes more complex.

Below, based on the Laplace vector and the angular momentum vector, we will present a new method for studying the secular evolution of the orbits of exoplanets with an arbitrary orbital orientation relative to the plane of the observer.

4.1 Two methods of setting problems for two-planet problems of extrasolar systems

With the discovery of planets around other stars [9], new trends have also appeared in the two-planet problem. Here we will consider exoplanetary systems for which the conditions of *small eccentricities and the angle of mutual inclination of the orbits are fulfilled*. In addition, for exoplanets there is another important geometric parameter — the angle of orientation of the orbit relative to the picture plane (the plane of the observer), see, for example, [10]. Currently, orbital elements for the overwhelming majority of exoplanets are found using the transit method, when the observer sees the orbits almost 'edge-on.' However, orbits more open relative to the observer's line of sight may also exist around stars, so when analyzing observational data, one must consider the selection effect: in the overwhelming majority of cases, it is the orbits seen almost 'edge-on' that are represented in the database on the NASA Exoplanet Archive service [9].

But with the improvement of observational methods, two-planet systems will be discovered (and the first examples already exist, see [11]) *in which the angle of inclination of the orbits to the picture plane is not necessarily close to* $\pi/2$ *but can be arbitrary*. And then the question inevitably arises: what method can be used to study the secular evolution of a system of two exoplanets *with an arbitrary angle* of inclination relative to the picture plane? Note that individual examples of two-planet systems with a large angle of mutual inclination of the orbits to the plane of the sky are sometimes discussed in the literature [12], but for such systems the additional condition of quasi-coplanarity of the orbits is not satisfied.

From a theoretical point of view, two-planet problems for extrasolar systems can be posed and studied in two ways:

1. Either we first transform the *coordinates of the orbit elements* from the image plane to the Laplace plane (or any other main plane), find a classical solution for orbits relative to the selected main plane, and then do the reverse coordinate transformation for this solution in the image plane;

2. *Or we directly derive the equations of the evolution of the elements of the orbit relative to the image plane and solve them already*. The second method is attractive because it significantly reduces the amount of numerical and theoretical calculations.

Next, we give an example of setting and solving the problem according to option 2.

4.2 Orbital orientation vectors

Let us consider the directional unit vectors of planetary orbits [2, 3]: the first of them is the vector $\mathbf{P}_j$ $(j = 1, 2)$, which is directed along the main axis of the ellipse to the pericenter

$$\mathbf{P}_j = \begin{pmatrix} P_{jx} \\ P_{jy} \\ P_{jz} \end{pmatrix} = \begin{pmatrix} \cos\omega_j \cos\Omega_j - \sin\omega_j \sin\Omega_j \cos i_j \\ \cos\omega_j \sin\Omega_j + \sin\omega_j \cos\Omega_j \cos i_j \\ \sin\omega_j \;\; \sin i_j \end{pmatrix}, \tag{4.2}$$

the second vector

$$\mathbf{Q}_j = \begin{pmatrix} Q_{jx} \\ Q_{jy} \\ Q_{jz} \end{pmatrix} = \begin{pmatrix} -\sin\omega_j \cos\Omega_j - \cos\omega_j \sin\Omega_j \cos i_j \\ -\sin\omega_j \sin\Omega_j + \cos\omega_j \cos\Omega_j \cos i_j \\ \cos\omega_j \;\; \sin i_j \end{pmatrix}, \tag{4.3}$$

perpendicular to the vector $\mathbf{P}_j$ lies in the plane of the ellipse and is directed along its minor axis; the third vector

$$\mathbf{R}_j = \begin{pmatrix} R_{jx} \\ R_{jy} \\ R_{jz} \end{pmatrix} = \begin{pmatrix} \sin i_j \sin\Omega_j \\ -\sin i_j \cos\Omega_j \\ \cos i_j \end{pmatrix}, \tag{4.4}$$

is perpendicular to the orbital plane.

Based on the unit vectors (4.2)–(4.4), we construct a system of three orientation vectors that determine the orientation of an elliptical orbit. First, there is the Laplace vector $\mathbf{L}_j = e_j \mathbf{P}_j$ whose absolute value is equal to the orbital eccentricity. The second vector $\mathbf{H}_j = e_j \mathbf{Q}_j$ (the Hamilton vector) is perpendicular to $\mathbf{L}_j$ and has the same absolute value. The third vector $\mathbf{l}_j = [1 - e_j^2]^{1/2}\, \mathbf{R}_j$ is the specific orbital angular momentum vector. This vector $\mathbf{l}_j$ is perpendicular to the vectors $\mathbf{L}_j$ and $\mathbf{H}_j$ therefore, to the orbital plane.

4.3 Secular evolution equations for orbit orientation vectors

For the vectors of two orbits $\mathbf{L}_j$, $\mathbf{H}_j$ and $\mathbf{l}_j$, using the Lagrange equations (3.1), we find the differential equations of motion in the linear approximation [12]:

$$\frac{\mathrm{d}\mathbf{L}_1}{\mathrm{d}t} = A_1 \mathbf{H}_1 - B_1 \mathbf{H}_2 \,, \quad \frac{\mathrm{d}\mathbf{H}_1}{\mathrm{d}t} = -(A_1 \mathbf{L}_1 - B_1 \mathbf{L}_2) \,,$$
$$\frac{\mathrm{d}\mathbf{l}_1}{\mathrm{d}t} = A_1 \, [\mathbf{l}_1 \times \mathbf{l}_2] \,. \tag{4.5}$$

$$\frac{\mathrm{d}\mathbf{L}_2}{\mathrm{d}t} = A_2 \mathbf{H}_2 - B_2 \mathbf{H}_1 \,, \quad \frac{\mathrm{d}\mathbf{H}_2}{\mathrm{d}t} = -(A_2 \mathbf{L}_2 - B_2 \mathbf{L}_1) \,,$$
$$\frac{\mathrm{d}\mathbf{l}_2}{\mathrm{d}t} = A_2 \, [\mathbf{l}_2 \times \mathbf{l}_1] \,. \tag{4.6}$$

Equations (4.5) and (4.6) represent two independent groups of differential equations. For the coefficients, we use the following notation:

$$A_1 = \frac{n_1 m_2}{2M}\, A \,, \quad B_1 = \frac{n_1 m_2}{2M}\, B \,,$$
$$A_2 = \frac{n_2 m_1 \alpha}{2M}\, A \,, \quad B_2 = \frac{n_2 m_1 \alpha}{2M}\, B \,, \tag{4.7}$$

having the dimension of frequency of oscillations, where

$$A = \frac{1}{\pi(1+\alpha)} \left[\frac{1+\alpha^2}{(1-\alpha)^2}\, E\left(\frac{2\sqrt{\alpha}}{1+\alpha}\right) - K\left(\frac{2\sqrt{\alpha}}{1+\alpha}\right) \right],$$
$$B = \frac{2}{\pi\alpha(1+\alpha)} \left[\frac{1-\alpha^2+\alpha^4}{(1-\alpha)^2}\, E\left(\frac{2\sqrt{\alpha}}{1+\alpha}\right) \right.$$
$$\left. - (1+\alpha^2)\, K\left(\frac{2\sqrt{\alpha}}{1+\alpha}\right) \right], \quad \alpha = \frac{a_2}{a_1} \,. \tag{4.8}$$

4.4 Solving evolution equations

The solutions of the linear equations (4.5) and (4.6) have the form [12]

$$\mathbf{L}_1^{(1)}(t) = D\big(\mathbf{C}_1^{(1)} \cos(g_1 t) + \mathbf{C}_2^{(1)} \sin(g_1 t)\big)$$
$$+ B_1 \big(\mathbf{C}_3^{(1)} \cos(g_2 t) + \mathbf{C}_4^{(1)} \sin(g_2 t)\big) \,,$$
$$\mathbf{L}_2^{(1)}(t) = B_2 \big(\mathbf{C}_1^{(1)} \cos(g_1 t) + \mathbf{C}_2^{(1)} \sin(g_1 t)\big)$$
$$- D\big(\mathbf{C}_3^{(1)} \cos(g_2 t) + \mathbf{C}_4^{(1)} \sin(g_2 t)\big) \,, \tag{4.9}$$

$$\begin{aligned}
\mathbf{H}_1^{(1)}(t) &= D\big(-\mathbf{C}_1^{(1)}\sin(g_1 t)+\mathbf{C}_2^{(1)}\cos(g_1 t)\big)\\
&\quad + B_1\big(-\mathbf{C}_3^{(1)}\sin(g_2 t)+\mathbf{C}_4^{(1)}\cos(g_2 t)\big)\,,\\
\mathbf{H}_2^{(1)}(t) &= B_2\big(-\mathbf{C}_1^{(1)}\sin(g_1 t)+\mathbf{C}_2^{(1)}\cos(g_1 t)\big)\\
&\quad - D\big(-\mathbf{C}_3^{(1)}\sin(g_2 t)+\mathbf{C}_4^{(1)}\cos(g_2 t)\big)\,, \qquad (4.10)
\end{aligned}$$

$$\begin{aligned}
\mathbf{l}_1^{(1)}(t) &= \mathbf{C}_1^0 + A_1\big(\mathbf{C}_5^{(1)}\cos(gt)+\mathbf{C}_6^{(1)}\sin(gt)\big)\,,\\
\mathbf{l}_2^{(1)}(t) &= \mathbf{C}_2^0 - A_2\big(\mathbf{C}_5^{(1)}\cos(gt)+\mathbf{C}_6^{(1)}\sin(gt)\big)\,. \qquad (4.11)
\end{aligned}$$

These solutions of the evolutionary equations include coefficients

$$\begin{aligned}
&K^e = (A_1-A_2)^2 + 4B_1B_2\,, \quad \kappa=\sqrt{K^e}\,, \quad \sigma = A_1 + A_2\,,\\
&g_1 = \frac{\sigma-\kappa}{2}\,, \quad g_2 = \frac{\sigma+\kappa}{2}\,,\\
&D = \frac{A_2 - A_1 + \kappa}{2} = A_2 - g_1 = -(A_1 - g_2)\,,\\
&D^2 + B_1B_2 = \frac{\kappa^2 + (A_2-A_1)\kappa}{2} = \kappa D\,,\\
&\mathbf{C}_1^{(1)} = \frac{D\mathbf{L}_{10} + B_1\mathbf{L}_{20}}{\kappa D}\,; \quad \mathbf{C}_2^{(1)} = \frac{D\mathbf{H}_{10} + B_1\mathbf{H}_{20}}{\kappa D}\,;\\
&\mathbf{C}_3^{(1)} = -\frac{D\mathbf{L}_{20} - B_2\mathbf{L}_{10}}{\kappa D}\,; \quad \mathbf{C}_4^{(1)} = -\frac{D\mathbf{H}_{20} - B_2\mathbf{H}_{10}}{\kappa D}\,, \qquad (4.12)
\end{aligned}$$

$$g = \sqrt{A_1^2(\mathbf{l}_{10}\cdot\mathbf{l}_{10}) + A_2^2(\mathbf{l}_{20}\cdot\mathbf{l}_{20}) + 2A_1A_2(\mathbf{l}_{10}\cdot\mathbf{l}_{20})}\,. \qquad (4.13)$$

4.5 Application of the new method 2 to the two-planet exosystem HD 206893

The HD206893 system is interesting because its orbital orientation (see the angle of inclination i in Table 1) differs significantly from the orientation of the orbits of exoplanets observed by the transit method. The data from [11] are presented in Table 1.

The solutions for the Laplace vector components and the specific orbital angular momentum are shown in Fig. 1 and 2.

The graphs of the Laplace vector hodograph can be seen in Fig. 3.

The evolution of the orbital elements calculated based on solutions (4.9)–(4.12) is shown in Fig. 4.

The oscillation periods in the HD 206893 system are shown in Table 2.

5. Gaussian ring and its potential

Another important direction originates from the Kepler ellipses — these are *Gauss rings*. In 1818, to calculate secular perturbations, Gauss proposed averaging the motion of the perturbing mass m along an orbital ellipse

$$r = \frac{p}{1+e\cos\upsilon}\,, \quad p = a(1-e^2)\,, \qquad (5.1)$$

where υ is the angle of the true anomaly. With this averaging, a material elliptical ring is formed with a density the greater the longer the body is in motion on the corresponding arc

Table 1. Data from the article [11] on the extrasolar system HD 206893. The mass of the central star is $M_* = 1.32^{+0.07}_{-0.05} M_\odot$, component b is a brown dwarf, component c is a hot Jupiter. The solutions for the components of the Laplace vector and the specific orbital angular momentum are shown in Fig. 1 and 2 [12].

Planet	M, M_{Jup}	a, a.u.	e	i, deg	ω, deg	Ω, deg
HD206893c	$12.7^{+1.2}_{-1.0}$	$3.53^{+0.08}_{-0.06}$	$0.41^{+0.03}_{-0.03}$	$150.9^{+2.9}_{-3.0}$	46^{+8}_{-8}	$89.1^{+6.9}_{-7.0}$
HD206893b	$28.0^{+2.2}_{-2.1}$	$9.6^{+0.4}_{-0.3}$	$0.14^{+0.05}_{-0.05}$	$146.8^{+3.3}_{-3.9}$	183^{+10}_{-10}	$73.5^{+5.0}_{-3.4}$

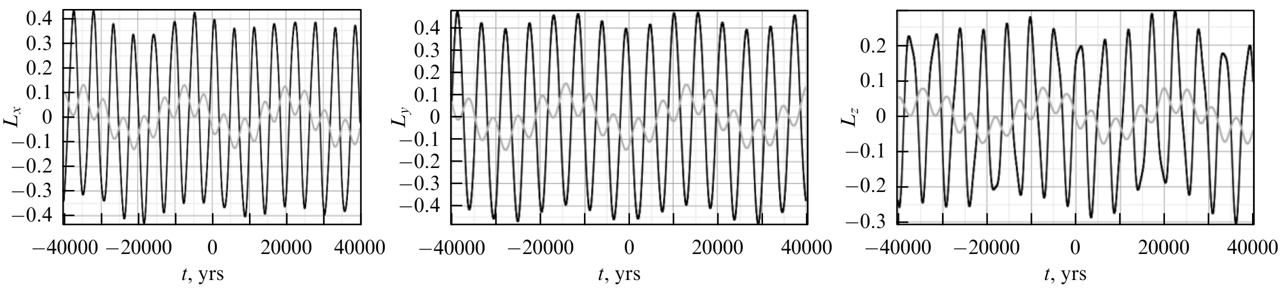

Figure 1. Oscillations of the components of the Laplace vectors over an interval of 80 thousand years for the components of the HD 206893 system (b — in gray, c — in black).

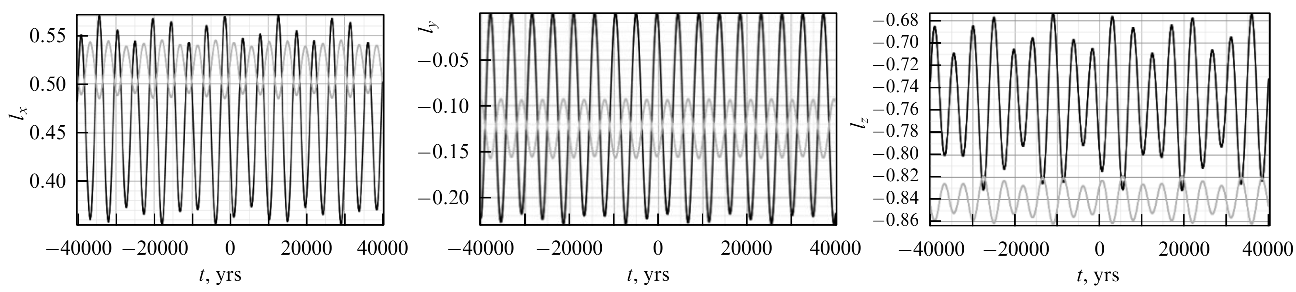

Figure 2. Oscillations of the components of specific orbital angular momenta over an interval of 80 thousand years for the components of the HD 206893 system (b — in gray, c — in black).

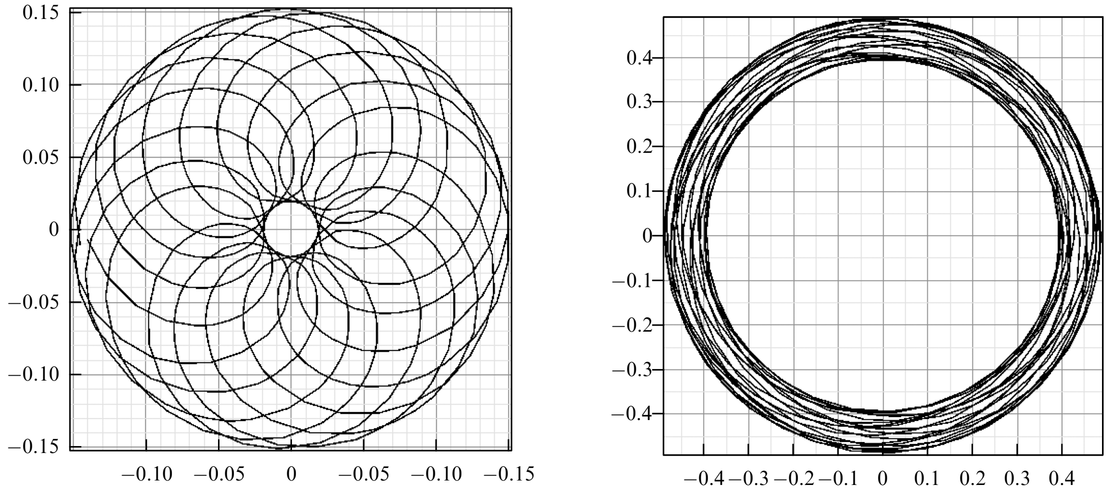

Figure 3. Hodograph of the Laplace vectors relative to the line of nodes in the plane perpendicular to the orbital angular momentum of the corresponding orbit, for the components of the HD 206893 system (b — left, c — right) over an interval of 114 thousand years.

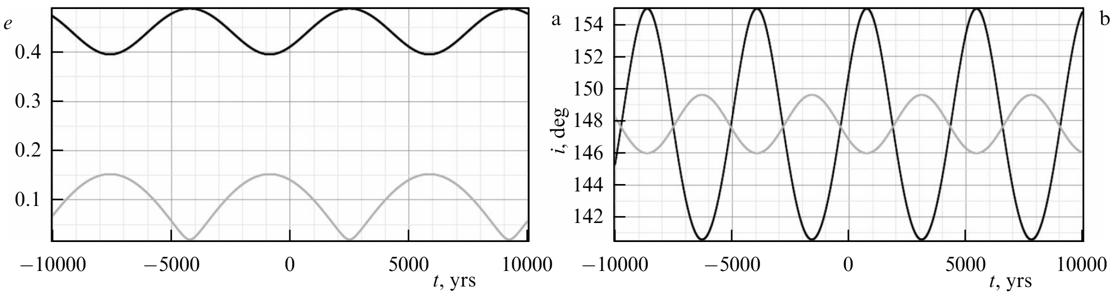

Figure 4. Evolution of the eccentricities (a) and inclinations (b) of the orbits of the components in HD 206893.

Table 2. Periods of the main oscillation frequencies in the two-planet problem for the HD 206893 system.

T_{g1}, yrs	T_{g2}, yrs	T_{κ}, yrs	T_{σ}, yrs	T_g, yrs
28400	5400	6700	4600	4700

(Fig. 5). The mass element $\mathrm{d}m$ on the ring in the angular interval $\mathrm{d}\upsilon$ is equal to

$$\mathrm{d}m = m\,\frac{(1-e^2)^{3/2}}{2\pi}\,\frac{\mathrm{d}\upsilon}{(1+e\cos\upsilon)^2}\,.$$

As a result, the problem of calculating perturbations in the first order is reduced to finding the gravitational influence of the Gauss ring on the external body.

5.1 Gaussian ring potential

Knowledge of the Gaussian ring potential is of central importance. In integral form, this potential is equal

$$\varphi_r(x) = \frac{mG(1-e^2)^{3/2}}{2\pi} \times \int_0^{2\pi} \frac{\mathrm{d}\upsilon}{(1+e\cos\upsilon)\sqrt{A_0+A_1\cos\upsilon+A_2\sin\upsilon+A_3\cos^2\upsilon+A_4\sin\upsilon\cos\upsilon}} \qquad (5.2)$$

(the coefficients A_i depend on the coordinates of the test point). This integral cannot be taken in general form; Gauss also did not find the potential of the ring. However, this potential is now known in analytical form, and it was

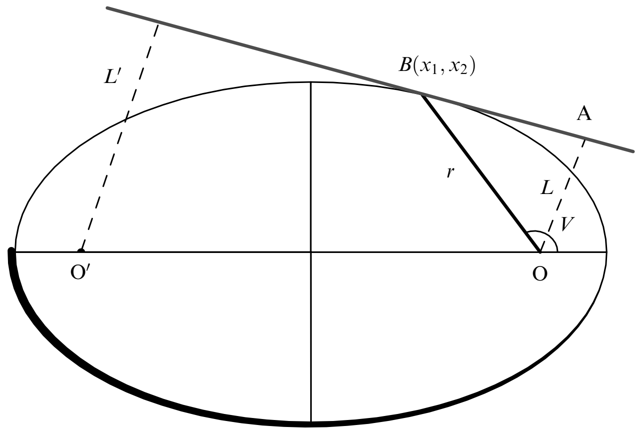

Figure 5. Auxiliary geometric elements for constructing a generalized flat homeoid with the homothetical center in focus O. The lower half of the ring shows its heterogeneity. (Notes in the text.)

obtained using new methods of the potential theory [14]. The secret is that the Gauss ring can be represented as a *generalized two-dimensional homothetic layer*.

Recall that a classical flat homeoid is a shell bounded by two concentric similar ellipses, and its homothetic center is located in the center of the ellipse. But in the *generalized homeoid, the homothetic center is already in the focus of the ellipse* O (Fig. 5).

According to the property of the generalized homeoid, the thickness of the layer at a point $B(x_1, x_2)$ must be proportional to the length of the segment $\mathrm{OA} = L$ equal to the shortest distance from the focal point to the tangent at the point $B(x_1, x_2)$. Such a layer, as can be shown, is indeed determined by the thickness

$$\mathrm{d}\tau = \frac{\mathrm{d}m}{m} = \frac{(1-e^2)^{3/2}}{2\pi} \frac{\mathrm{d}\upsilon}{(1+e\cos\upsilon)^2}\,, \tag{5.3}$$

characterizing exactly the Gaussian ring. Moreover, with this approach, we come to another important conclusion: it turns out that the potential of a Gaussian ring φ_r will be related to the potential of the initial homogeneous elliptical disk φ_d by equation [14]

$$\begin{aligned}\varphi_r(\mathbf{x}) &= \frac{1}{2}\left(\varphi_d(\mathbf{x}) - \mathbf{x}\boldsymbol{\nabla}\varphi_d\right)\\ &= \frac{1}{2}\left(\varphi_d(\mathbf{x}) - x_1\frac{\partial\varphi_d}{\partial x_1} - x_2\frac{\partial\varphi_d}{\partial x_2} - x_3\frac{\partial\varphi_d}{\partial x_3}\right).\end{aligned} \tag{5.4}$$

According to the theory of equigravitating bodies [14], the potential of a homogeneous elliptical disk φ_d is obtained through the potential of an inhomogeneous ellipsoid φ_{el} with a density distribution

$$\begin{aligned}&r = \frac{r_0}{\sqrt{1-m^2}}\,, \quad m^2 = \frac{x_1^2}{a_1^2} + \frac{x_2^2}{a_2^2} + \frac{x_3^2}{a_3^2}\,, \quad 0 \leqslant m \leqslant 1\,,\\ &\varphi_{el} = 2\pi G\rho_0 a_1 a_2 a_3\\ &\times \int_\lambda^\infty \frac{\sqrt{1 - x_1^2/(a_1^2+u) - x_2^2/(a_2^2+u) - x_3^2/(a_3^2+u)}}{\sqrt{(a_1^2+u)(a_2^2+u)(a_3^2+u)}}\,\mathrm{d}u.\end{aligned} \tag{5.5}$$

This is proved using a special method of confocal 'compression' of the mass by hyperbolas: then a homogeneous elliptical disk is obtained from an inhomogeneous triaxial ellipsoid (Fig. 6). This inhomogeneous triaxial ellipsoid and a homogeneous elliptical disk turn out to be equigravitating (having the same potentials) in the external space. As a result, through the potential of the ellipsoid (5.5), equal to (see [14])

$$\begin{aligned}\varphi_{el}(\mathbf{x}) = \varphi_d(\mathbf{x}) &= \frac{4G\sigma a_1 a_2}{\sqrt{\lambda - v}}\left\{\frac{x_1 + ea_1}{a_1^2 + v}\,\Pi\left[-\frac{a_1^2+v}{\lambda - v}, k\right]\right.\\ &\left. + \frac{x_2^2}{a_2^2+v}\,\Pi\left[-\frac{a_2^2+v}{\lambda - v}, k\right] + \frac{x_3^2}{v}\,\Pi\left[-\frac{v}{\lambda-v}, k\right]\right\},\\ k &= \sqrt{\frac{\mu - v}{\lambda - v}} \leqslant 1\,,\end{aligned} \tag{5.6}$$

we also find the potential of a homogeneous elliptical disk. Substituting expression (5.6) into the right-hand side of formula (5.4), we ultimately obtain the potential of the Gaussian ring in analytical form [15]

$$\begin{aligned}\varphi_{\mathrm{ring}}(x_1, x_2, x_3) &= \frac{2Gm}{\pi\sqrt{\lambda - v}}\\ &\times\left\{K(k) + \frac{ea(x_1 + ea)}{a^2 + v}\left[\Pi(n,k) - K(k)\right]\right\},\\ n = \frac{a^2+v}{v - \lambda}\,, \quad & k = \sqrt{\frac{\mu - v}{\lambda - v}} \leqslant 1\,.\end{aligned} \tag{5.7}$$

where m is the mass of the ring, a and b — its major and minor semi-axes, and e — its eccentricity. $K(k)$ and $\Pi(n,k)$ are the standard complete elliptic Legendre integrals of the first and third kind. Figure 7 shows the family of equipotentials of the Gauss ring.

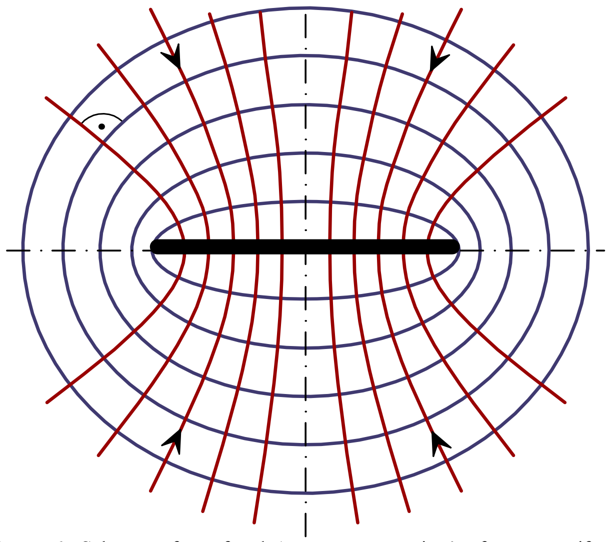

Figure 6. Scheme of confocal 'mass compression' of a nonuniform ellipsoid along hyperbolas, transforming the ellipsoid into a uniform elliptical disk (shown in bold).

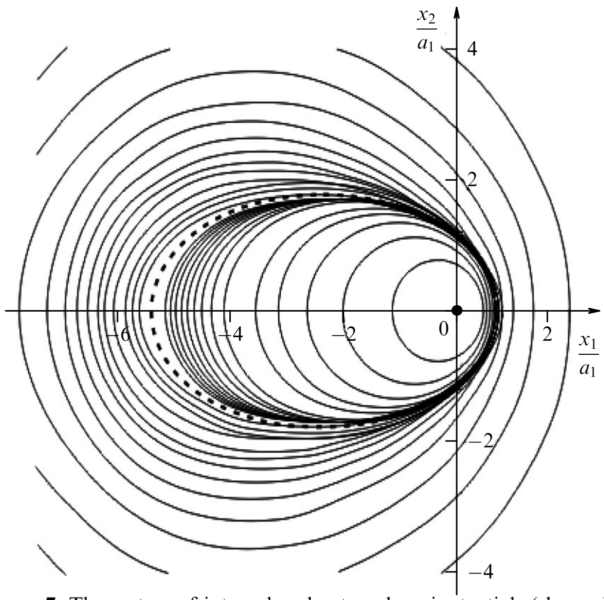

Figure 7. The system of internal and external equipotentials (shown by continuous curves) in the plane of the Gaussian ring. The ring itself is shown as a dotted line. At the point of the right focus (the center of the homothetic ring, marked with a bold dot), the potential has a minimum $\varphi(0,0,0) = 2Gm/a$ inside the ring. On the ring itself, the potential diverges logarithmically. (According to the article [15].)

5.2 Systems of two Gaussian rings. The mutual gravitational energy of these rings

With the development of the averaging method, systems of Gaussian rings began to be studied. A new approach to the study of long-period and secular perturbations in some problems of celestial mechanics was developed at the Sternberg Astronomical Institute on the basis of ring systems [16, 17]. In this approach, we rely not on the standard Lagrange perturbation function R but on the mutual potential energy W_{mut} of Gauss rings

$$\begin{aligned}W_{\mathrm{mut}} &= -\frac{Gm_1m_2(1-e_1^2)^{3/2}(1-e_2^2)^{3/2}}{4\pi^2}\int_0^{2\pi}\int_0^{2\pi}\frac{1}{r_{12}}\\ &\times\frac{\mathrm{d}\upsilon_1}{(1+e_1\cos\upsilon_1)^2}\,\frac{\mathrm{d}\upsilon_2}{(1+e_2\cos\upsilon_2)^2}\,,\end{aligned} \tag{5.8}$$

where r_{12} is the distance between two points on the rings.

Assuming that the eccentricities of the rings (e_1, e_2) and the angle Δi of their mutual inclination are small, we decompose the integral expression in (5.8) according to the powers of these small parameters into a triple Taylor series up to terms of the fourth degree. After integrating this series, the expression for the mutual energy is represented as [16]

$$W_{\rm mut} = -\frac{Gm_1m_2}{\pi a_1}\Big\{W_{000} + W_{200}(e_1^2 + e_2^2 - \Delta i^2) + W_{110}\,e_1e_2 + W_{400}\,e_1^4 + W_{310}\,e_1^3e_2 + W_{220}\,e_1^2e_2^2 + W_{130}\,e_1e_2^3 + W_{040}\,e_2^4 + \Delta i^2\big[W_{202}\,e_1^2 + W_{022}\,e_2^2 + W_{112}\,e_1e_2\big] + W_{004}\,\Delta i^4\Big\}. \quad (5.9)$$

The coefficients W_{klm} in expression (5.9) for the mutual energy of Gauss rings were obtained in the final form using Legendre elliptic integrals [16].

6. Problem of confinement of rings around small bodies in the Solar system

6.1 Nonplanetary type rings around small bodies

Rings around celestial bodies have long attracted the attention of researchers. For an overview of the history of this issue from Newton to 1990, see the book by Friedman and Gorkavy [18], where the rings around the four giant planets of the Solar System were studied. The sharp edges of the rings were explained there by the mechanism of particle collisions and the resonance of particle orbits with shepherd satellites.

After the recent discovery of rings around small celestial bodies (the asteroid Centaur Chariclo [19] and two Kuiper Belt objects, Haumea [20, 21] and Quaoar [22]), interest in ring dynamics has increased even more. These rings differ from planetary-type rings: they are narrow, can be located outside the Rocha boundary of the central celestial body, and do not have shepherd satellites. It is also interesting that the motion of ring particles around small bodies is often in spin-orbit resonance 3:1 with the central body. Therefore, the problem of describing the secular evolution of such rings and creating new mechanisms for their stabilization is very acute now. To solve the retention problem, we will consider the self-gravity mechanism of the rings.

To implement the self-gravitation mechanism of the rings, we apply the model of two Gaussian rings [23]. The confinement problem of ring is complex and is solved here in several stages. In the first stage, a model of a composite ring is created, where a narrow 2D ring is represented by a system of two close Gaussian rings. A necessary condition for stabilizing the shape of the composite ring is to take into account its self-gravitation through the mutual energy of the boundary rings $W_{\rm mut}$. The function $W_{\rm mut}$ is represented in (5.9) by a series up to terms of the 4th degree of smallness.

In the problem with rings, it should also be taken into account that the central ellipsoid with semi-axes $a_1 > a_2 > a_3$ rapidly rotates around the minor axis, therefore, to study the secular effects in the motion of ring particles, it is necessary to average the ellipsoid potential over the azimuthal angle λ in the interval (0.2π). After averaging, the potential will take the form [23]

$$\varphi(r,z) \approx \frac{GM}{r}\left[1 + \frac{1}{2}\,C_{20}\left(\frac{R_0}{r}\right)^2\left(3\left(\frac{z}{r}\right)^2 - 1\right) + \frac{1}{8} \times C_{40}\left(\frac{R_0}{r}\right)^4\left(35\left(\frac{z}{r}\right)^4 - 30\left(\frac{z}{r}\right)^2 + 3\right)\right], \quad (6.1)$$

where z is the height of the test particle above the plane of the conventional equator. The zonal coefficients C_{20} and C_{40} in potential (6.1) are equal to:

$$C_{20} = \frac{2a_3^2 - a_1^2 - a_2^2}{10R_0^2}\,,$$
$$C_{40} = 3\,\frac{3(a_1^4 + a_2^4) + 8a_3^4 + 2a_1^2a_2^2 - 8\,(a_1^2 + a_2^2)\,a_3^2}{280R_0^4}. \quad (6.2)$$

6.2 Evolution equations for two rings in collective variables in the central field

In collective variables [23], we obtain a system of 8 differential equations ring evolutions in the central (index c) field:

$$\left(\frac{d\Delta\omega}{dt}\right)_c = -\frac{3}{16}\,C_{20}\,n\left(\frac{R}{a}\right)^2\left[20\,(\cos^2 i_2 - \cos^2 i_1) - 7\,\frac{\Delta a}{a}\,\big(5\,(\cos^2 i_2 + \cos^2 i_1) - 2\big)\right], \quad (6.3)$$

$$\left(\frac{d\omega}{dt}\right)_c = -\frac{3}{8}\,C_{20}\,n\left(\frac{R}{a}\right)^2\left[5\,(\cos^2 i_2 + \cos^2 i_1) - 2 - \frac{35}{4}\,\frac{\Delta a}{a}\,(\cos^2 i_2 - \cos^2 i_1)\right], \quad (6.4)$$

$$\left(\frac{d\Delta e}{dt}\right)_c = -\frac{15}{32}C_{40}n\left(\frac{R}{a}\right)^4\big(\sin^2 i_1\sin 2\omega_1(7\cos^2 i_1 - 1) \times e_1 - \sin^2 i_2\sin 2\omega_2\,(7\cos^2 i_2 - 1)e_2\big)\,, \quad (6.5)$$

$$\left(\frac{de}{dt}\right)_c = -\frac{15}{64}C_{40}n\left(\frac{R}{a}\right)^4\big(\sin^2 i_1\sin 2\omega_1(7\cos^2 i_1 - 1) \times e_1 + \sin^2 i_2\sin 2\omega_2\,(7\cos^2 i_2 - 1)e_2\big)\,, \quad (6.6)$$

$$\left(\frac{d\Delta\Omega}{dt}\right)_c = -\frac{3}{8}\,C_{20}\,n\left(\frac{R}{a}\right)^2\left[4\,(\cos i_1 - \cos i_2) - 7\,\frac{\Delta a}{a}\,(\cos i_1 + \cos i_2)\right], \quad (6.7)$$

$$\left(\frac{d\Omega}{dt}\right)_c = -\frac{3}{16}\,C_{20}\,n\left(\frac{R}{a}\right)^2\left[4\,(\cos i_1 + \cos i_2) - 7\,\frac{\Delta a}{a}\,(\cos i_1 - \cos i_2)\right], \quad (6.8)$$

$$\left(\frac{d\Delta i}{dt}\right)_c = \frac{15}{64}\,C_{40}\,n\left(\frac{R}{a}\right)^4\Big[\sin 2i_1\sin 2\omega_1(7\cos^2 i_1 - 1)\,e_1^2 - \sin 2i_2\sin 2\omega_2(7\cos^2 i_2 - 1)\,e_2^2 + \frac{11}{4}\,\frac{\Delta a}{a} \times \big(\sin 2i_1\sin 2\omega_1(7\cos^2 i_1 - 1)\,e_1^2 + \sin 2i_2\sin 2\omega_2(7\cos^2 i_2 - 1)\,e_2^2\big)\Big], \quad (6.9)$$

$$\left(\frac{di}{dt}\right)_c = -\frac{15}{128}C_{40}\,n\left(\frac{R}{a}\right)^4\Big[\sin 2i_1\sin 2\omega_1(7\cos^2 i_1 - 1)\,e_1^2 + \sin 2i_2\sin 2\omega_2(7\cos^2 i_2 - 1)\,e_2^2 + \frac{11}{4}\,\frac{\Delta a}{a} \times \big(\sin 2i_1\sin 2\omega_1(7\cos^2 i_1 - 1)\,e_1^2 - \sin 2i_2\sin 2\omega_2(7\cos^2 i_2 - 1)\,e_2^2\big)\Big]. \quad (6.10)$$

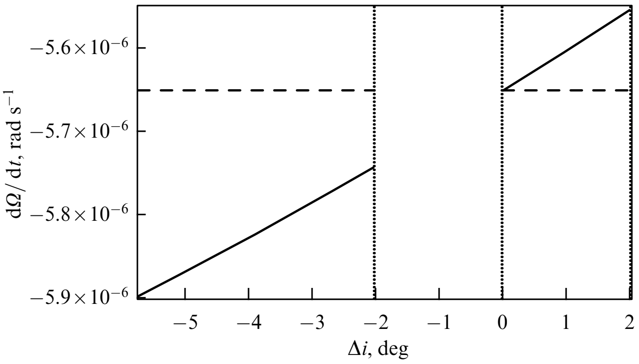

Figure 8. Precession of the nodes $\mathrm{d}\Omega/\mathrm{d}t$ of the Haumea ring in the equatorial plane of the central body depending on the difference in the angles of inclination Δi of the boundaries of this ring. The horizontal dashed line indicates the value of the angular velocity without taking into account the self-gravity of the ring (which gives $T_\Omega = 12.9 \pm 0.7$ d). Taking into account the self-gravity of the ring, the results of the calculations are shown by the inclined line in the upper right rectangle. (According to the work [23].)

For example, these equations were used to calculate the nodal precession of the Haumea ring relative to the plane of its equator [23]. The results of the calculations are shown in Fig. 8.

According to Fig. 8, taking into account self-gravity actually reduces the time of nodal precession of the ring.

6.3 Ring stabilization conditions

For coplanar elliptical rings, neglecting the inclination of Haumea's ring to the equatorial plane, the confinement conditions are [23]:

$$\left(\frac{\mathrm{d}\Delta e}{\mathrm{d}t}\right)_r + \left(\frac{\mathrm{d}\Delta e}{\mathrm{d}t}\right)_c = 0\,,$$
$$\left(\frac{\mathrm{d}\Delta\bar\omega}{\mathrm{d}t}\right)_r + \left(\frac{\mathrm{d}\Delta\bar\omega}{\mathrm{d}t}\right)_c = 0\,. \qquad (6.11)$$

The stability criterion for coplanar elliptical rings is $\Delta\bar\omega = 0$ that is, the apsidal lines of the bordering rings must coincide. For inclined rings, such a criterion is the coincidence of nodal lines.

6.4 Restriction on Haumea ring mass

According to equations (6.3)–(6.10), the reduced mass of the ring should depend on the eccentricities of the boundary ringlets (Fig. 9).

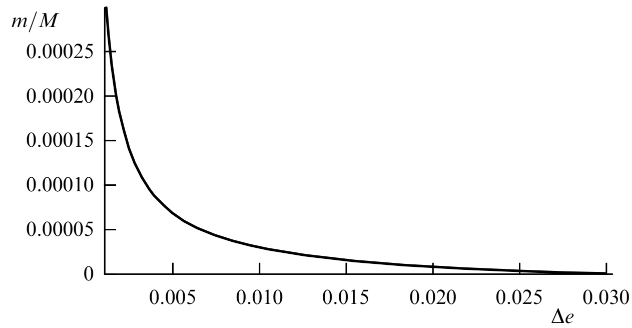

Figure 9. The dependence of the m/M ratio of the mass of the Haumea ring to the mass of the Haumea planetoid on the difference Δe in the eccentricities of the boundaries of this ring. (According to the article [23].)

As a result, we find that the normalized mass of the Haumea ring must satisfy the inequalities

$$10^{-4} < \frac{m}{M} < 10^{-3}\,. \qquad (6.12)$$

7. Two-dimensional generalization of the precessing Gaussian ring (R-disk model)

According to the laws of celestial mechanics, external disturbances and the effects of general relativity cause apsidal precession of an elliptical Gaussian ring. As a result [14, 24, 25], azimuthal averaging yields an R-disk (or R-ring). Such R-disks are formed either: (a) from many single Gaussian rings whose apsidal lines are uniformly distributed over the azimuthal angle, (b) or by rosette-shaped orbits precessing around a central mass (Fig. 10). The usefulness of this model is determined by the fact that such R-rings can naturally form in planetary systems and in the central regions of flat galaxies.

7.1 The R-ring structure

We rely on the works [24, 25]. Classical integral in the two-body problem is

$$V^2 = GM\left(\frac{2}{r} - \frac{1}{a}\right). \qquad (7.1)$$

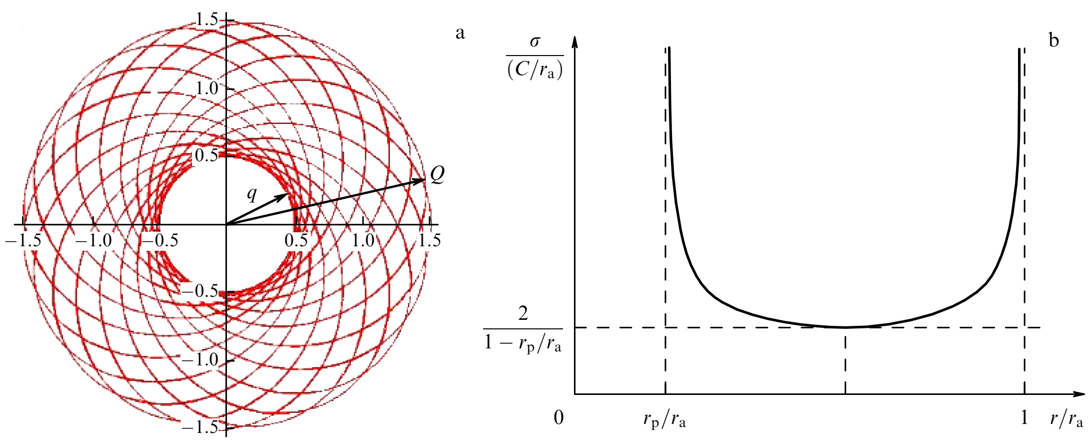

Figure 10. On the left is an R-ring filled with a rosette orbit; on the right is the density in the R-ring as a function of the normalized radius of the point. (According to the article [25].)

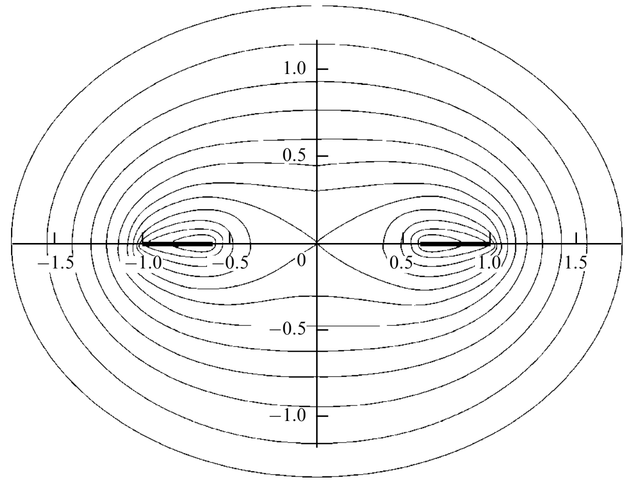

Figure 11. Equipotentials of the R-ring in the main plane. The cross-section of the ring is shown by the thick line [14].

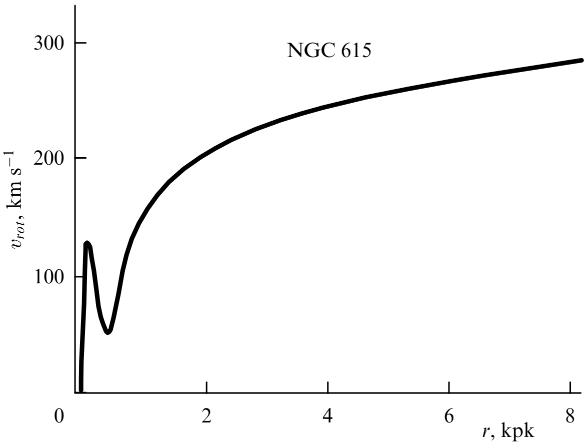

Figure 12. The rotation curve of NGC 615 galaxy as a typical example of the rotation profile of flat galaxies with a sharp local minimum.

Since the motion is planar $V^2 = V_r^2 + V_\theta^2$ we eliminate the azimuthal component of the velocity using the angular momentum of the particle $rV_\theta = \sqrt{GMa\,(1-e^2)}$. Then, the radial component of the velocity is

$$V_r = V_0\,\frac{\sqrt{(Q-r)(r-q)}}{r}\,. \tag{7.2}$$

In a narrow ring at a distance $(r, r + \mathrm{d}r)$ from the attracting body, the body is in the time interval

$$\mathrm{d}t = \frac{r\,\mathrm{d}r}{V_0\sqrt{(Q-r)(r-q)}}\,. \tag{7.3}$$

Therefore, the probability of finding a body in a narrow ring is equal to

$$\mathrm{d}\omega = \frac{2\,\mathrm{d}t}{T} = \frac{r\,\mathrm{d}r}{\pi a\sqrt{(Q-r)(r-q)}}\,. \tag{7.4}$$

The mass of the narrow ring is

$$\mathrm{d}M = 2\pi r\sigma(r)\,\mathrm{d}r\,, \tag{7.5}$$

so that the density distribution in the R-ring will be

$$\sigma = \frac{C}{\sqrt{(Q-r)(r-q)}}\,,\qquad C = \frac{M}{\pi^2(Q+q)}\,. \tag{7.6}$$

It can be seen that the density at the inner and outer circular boundaries of the R-ring has a peculiarity.

7.2 R-ring potential

The 3D potential of the R-ring is given by the integral [14, 24, 25]

$$\varphi(r, x_3) = 4GC\int_{-\pi/2}^{\pi/2}\frac{R-r}{\sqrt{R^2+x_3^2}}\,K\left(\sqrt{\frac{4r(R-r)}{R^2+x_3^2}}\right)\mathrm{d}\gamma\,,$$
$$R = \frac{Q-q}{2}\sin\gamma + \frac{Q+q}{2} + r\,. \tag{7.7}$$

The results of calculation using formula (7.7) are shown in Fig. 11.

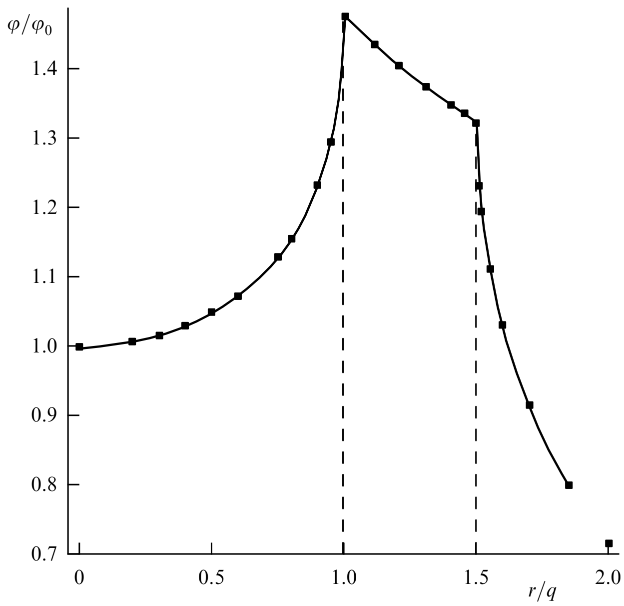

Figure 13. Potential of the R-disk in the principal plane. The vertical lines mark the entrance and exit of the disk [25].

7.3 Applying the R-ring model

The R-ring model has been applied to several problems. We will mention two of them here.

7.3.1 Explanation of sharp local minima on galaxy rotation curves. In the first problem [25], the model allowed us to explain the reason for the existence of sharp local minima on the rotation curves of some flat galaxies (Fig. 12).

Rotation curve of the galaxy NGC 615 as a typical example of the rotation profile of flat galaxies. Calculations have shown that in the cavity of the R-ring — from the center to the inner boundary — the potential increases (Fig. 13), and in this interval, an additional 'repulsive' force acts from the center. Then the potential decreases, and the additional force on the particles is directed toward the center. If such an R-ring is placed in the potential of a spherical (or spheroidal) bulge, this property of the R-ring's gravitational field can lead to a local decrease in the rotational velocity of the gas near q.

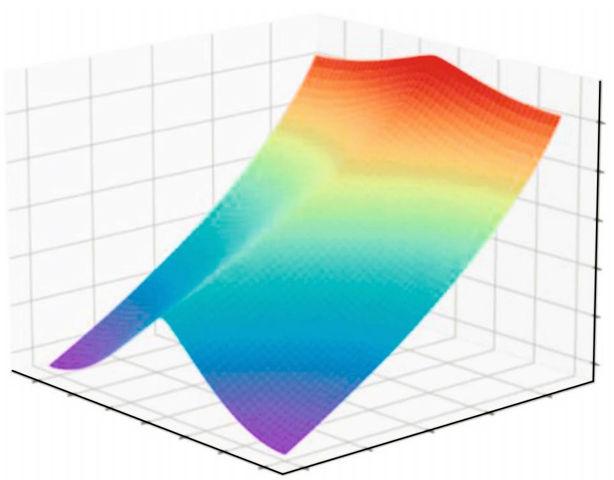

Figure 14. Three-dimensional dependence of the normalized mutual gravitational energy between the R-ring and the outer narrow circular ring on the inclination angle α (in rad) and the radius r_2 (in arc seconds). According to the article [26].

7.3.2 Dynamics of star disks in the central parsec of the Galaxy. In another problem [26], the R-ring model was used to study the characteristics of interacting stellar disks ('clockwise' and 'anticlockwise' disks) in the central parsec of the Galaxy. For this purpose, the mutual gravitational energy of the R-ring and the outer circular ring was found

$$W_{\mathrm{mut}}(r,\alpha) = -\frac{16GM_1M_2}{\pi^2(Q+q)\sqrt{r_2}}\int_0^{\pi/2}\int_q^Q \frac{\sqrt{r}}{\sqrt{(Q-r)(r-q)}} \times \frac{1}{m}K\left(\frac{2n^{1/4}}{m}\right)\mathrm{d}r\,\mathrm{d}\theta\,, \tag{7.8}$$

where

$$n = \sin^2\theta\cos^2\alpha + \cos^2\theta\,, \quad m = \sqrt{\frac{r^2+r_2^2}{rr_2} + 2\sqrt{n}}\,. \tag{7.9}$$

Knowing W_{mut}, we find the moment of force between two stellar rings

$$M = \frac{\partial W_{\mathrm{mut}}}{\partial\alpha}\,. \tag{7.10}$$

The results of calculating the moment of forces between the rings are shown in Fig. 15.

For the indicated stellar rings in the central parsec of the Galaxy, the moment of forces is equal to

$$M = -0.447\left(\frac{8GM_1M_2}{\pi^2\sqrt{a_1r_2}}\right). \tag{7.11}$$

Taking into account (7.11), using the formulas obtained earlier, we find the period of nodal precession of both stellar disks [26]

$$T_\Omega^{(2)} = T_\Omega^{(1)} = \frac{\pi^3\sqrt{GM_{\mathrm{bh}}a_1}r_2\sin\beta_1}{1.788GM_1} \approx 3.53\times10^5 \text{ yrs}\,, \tag{7.12}$$

where M_{bh} — the mass of the central black hole.

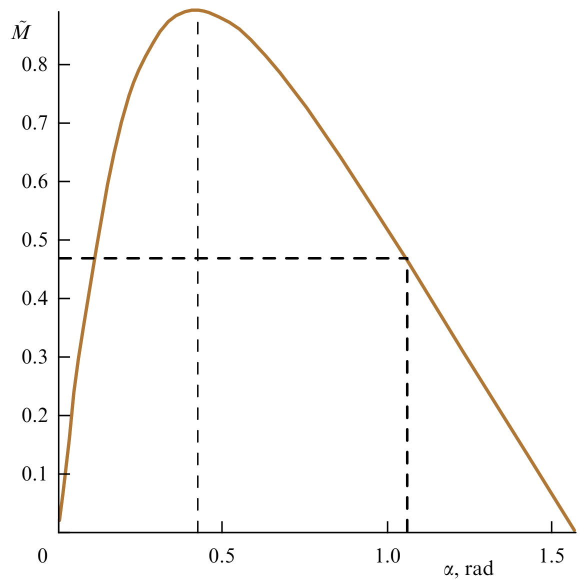

Figure 15. Dependence of the normalized moment of forces $\tilde{M} = M/(-8GM_1M_2/\pi^2\sqrt{a_1r_2})$ between the wide R-ring and the narrow ring on the angle of mutual inclination α. The curve has a maximum at $\alpha = 0.433(24.8^\circ)$. The position of the real 'disk 1–disk 2' system in the Galaxy $\alpha \approx 62^\circ$ is indicated by bold strokes.

8. Three-dimensional generalization of the precessing Gaussian ring (R-toroid model)

8.1 Geometry of the R-toroid figure

The Gaussian ring and its two-dimensional generalization (the R-ring) have already found application in modern dynamical astronomy. However, in practice, problems arise when the plane of the R-shaped ring itself precesses around a certain direction; this allows for another (additional) azimuth averaging of the satellite's orbit. The method for obtaining a new figure involves *triple averaging of the motion of a material point over 'fast' variables*: the first averaging yields a 1D Gaussian ring, the next step involves averaging the rotating Gaussian ring over the precession angle of its apsidal line, resulting in the R-ring; finally, the third step involves azimuthal averaging of the precessing R-ring, which ultimately yields a three-dimensional R-toroid [27–29]. The R-toroid figure is shown in Figs 16 and 17.

In spherical coordinates (r,θ,φ), the R-toroid figure is described by the constraints

$$q \leqslant r \leqslant Q\,, \quad -i \leqslant \theta \leqslant i\,. \tag{8.1}$$

8.2 Density and potential distribution in R-toroid

The density distribution inside the R-toroid [27, 28] is given by the formula

$$\rho(r,\theta) = \frac{M}{2\pi^3 ar\sqrt{\sin^2 i - \sin^2\theta}\sqrt{(Q-r)(r-q)}}\,. \tag{8.2}$$

According to (8.2), the surface of the R-toroid is a 'shell' with an anomalously high density. Indeed, for a given angle θ, the density (8.2) goes to infinity as on the outer (at $r = Q$) ABC and $A'B'C'$ (see Fig. 17), as well as on the internal (at $r = q$) abc and $a'b'c'$ frontal sections of the surface. The 'shell' appears not only due to the peculiarities of the density

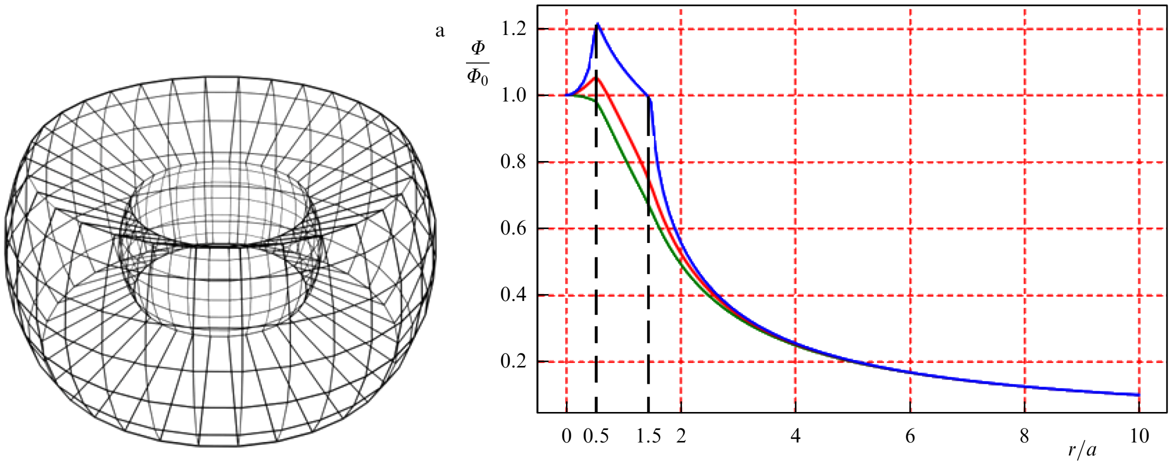

Figure 16. The figure of the R-toroid (a) and the dependence of its normalized potential in the equatorial plane (b). (According to the [27, 28].)

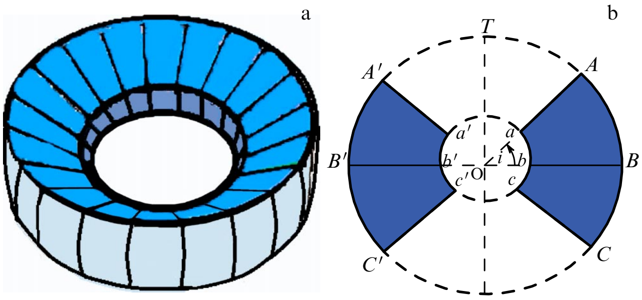

Figure 17. R-Toroid: on the left is 3D image, on the right is meridional section of the R-toroid (shown in blue). OT — the axis of symmetry. The outer (ABC and $A'B'C'$) and inner (abc and $a'b'c'$) boundaries on the right and left are parts of circles that are connected by straight line segments (aA, cC) and ($a'A', c'C'$). The angle of inclination i of the flat lateral sides is indicated.

distribution in the R-ring itself (see Fig. 10), but also due to the vanishing of the term $\sin^2 i - \sin^2\theta$ at points on the flat sides of the R-toroid itself.

Under the density law (8.2), the spatial potential of the R-toroid will be represented by a triple integral

$$\Phi(r,\theta,\varphi) = \frac{GM}{2\pi^3 ar}\int_0^{2\pi}\int_{-i}^{i}\int_q^Q \times \frac{r'\cos\theta'\,\mathrm{d}r'\,\mathrm{d}\theta'\,\mathrm{d}\varphi'}{\sqrt{\sin^2 i - \sin^2\theta}\sqrt{(Q-r)(r-q)}\sqrt{r^2+r'^2-2rr'\cos\Psi}}\,, \quad (8.3)$$

where Ψ is the angle between r and r' whose cosine is

$$\cos\Psi = \begin{pmatrix}\cos\varphi\cos\theta\\ \sin\varphi\cos\theta\\ \sin\theta\end{pmatrix}^T \begin{pmatrix}\cos\varphi'\cos\theta'\\ \sin\varphi'\cos\theta'\\ \sin\theta'\end{pmatrix} = \cos(\varphi'-\varphi)\cos\theta'\cos\theta + \sin\theta'\sin\theta\,, \quad (8.4)$$

The potential of the R-toroid in the equatorial plane is given by the double integral

$$\Phi(r,\theta) = \frac{GM}{2\pi^3 ar}\int_q^Q \frac{r'\,\mathrm{d}r'}{\sqrt{(Q-r)(r-q)}} \times \int_{-i}^{i}\frac{\cos\theta'\,\mathrm{d}\theta'}{\sqrt{\sin^2 i - \sin^2\theta}}\,\frac{K\big(2b_1/(b_1+b_2)\big)}{\sqrt{b_1+b_2}}\,, \quad (8.5)$$

where

$$b_1 = r^2 + r'^2\,, \quad b_2 = 2rr'\cos\theta'\,. \quad (8.6)$$

The potential of the R-toroid can also be represented in the form of series [27, 28]. So, in spherical coordinates, the expansion of the potential over small values of inverse distances (a/r) with an accuracy of terms of the 4th order has the form

$$\Phi(r,\theta) = \frac{GM}{r}\left\{1 - \frac{1}{2}\left(1+\frac{3}{2}e^2\right)P_2(\cos i)P_2(\sin\theta)\left(\frac{a}{r}\right)^2 + \frac{3}{8}\left(1+5e^2+\frac{15}{8}e^4\right)P_4(\cos i)P_4(\sin\theta)\left(\frac{a}{r}\right)^4\right\}. \quad (8.7)$$

8.3 Mutual energy of the R-toroid and the outer Gaussian ring. Equations of secular evolution of osculating orbits of bodies

The equations of the secular evolution of osculating orbits. To apply the model, it is necessary to know the expression of the mutual energy of the R-toroid and the outer Gauss ring [27, 28].

$$W_{\mathrm{mut}} = -\frac{GMM'}{a'}\left\{1 + \frac{1}{4(1-e'^2)^{3/2}}\left(1+\frac{3}{2}e^2\right) \times \bar P_2(\cos i)\bar P_2(\cos i')\left(\frac{a}{a'}\right)^2 + \frac{9}{64(1-e'^2)^{7/2}} \times \left(1+5e^2+\frac{15}{8}e^4\right)\bar P_4(\cos i)\left(\frac{a}{a'}\right)^4 \times \left[\left(1+\frac{1}{2}e'^2\right)\bar P_4(\cos i') + \frac{e'^2}{4}(5\cos^2 i' - 1) - \frac{5e'^2\sin^2 i'\sin^2 i'\sin^2\omega'}{4}(7\cos^2 i' - 1)\right]\right\}, \quad (8.8)$$

where $\bar P_2(x)$ and $\bar P_4(x)$ are Legendre polynomials of the 2nd and 4th degree.

Using (8.8) in [27, 28], a system of equations for the secular evolution of osculating orbits in the gravitational field of the R-toroid was obtained:

$$\left(\frac{\mathrm{d}e'}{\mathrm{d}t}\right)_p = \frac{15n'}{16}\, C_{40}^p\, \frac{M}{M_*}\left(\frac{a}{a'}\right)^4 \times \frac{\sin^2 i'(7\cos^2 i' - 1)e'\sin\omega'\cos\omega'}{(1-e'^2)^3}\,,$$
$$\left(\frac{\mathrm{d}i'}{\mathrm{d}t}\right)_p = -\frac{15n'}{16}\, C_{40}^p\, \frac{M}{M_*}\left(\frac{a}{a'}\right)^4 \times \frac{\sin i'\cos i'(7\cos^2 i' - 1)e'^2\sin\omega'\cos\omega'}{(1-e'^2)^4}\,, \quad (8.9)$$

$$\left(\frac{\mathrm{d}\Omega'}{\mathrm{d}t}\right)_p = \frac{3n'}{2}\, C_{20}^p\, \frac{M}{M_*}\left(\frac{a}{a'}\right)^2 \frac{\cos i'}{(1-e'^2)^2}\,,$$
$$\left(\frac{\mathrm{d}\omega'}{\mathrm{d}t}\right)_p = -\frac{3n'}{4}\, C_{20}^p\, \frac{M}{M_*}\left(\frac{a}{a'}\right)^2 \frac{5\cos^2 i' - 1}{(1-e'^2)^2}\,,$$

where M_* is the mass of the central star, M is the mass of the planet (R-toroid), and the coefficients of the zonal harmonics of the R-toroid field at the normalization radius $R = a$ are

$$C_{20}^p = -\frac{1}{2}\left(1 + \frac{3}{2}e^2\right)\bar{P}_2(\cos i)\,,$$
$$C_{40}^p = \frac{3}{8}\left(1 + 5e^2 + \frac{15}{8}e^4\right)\bar{P}_4(\cos i)\,. \quad (8.10)$$

9. Application of the R-toroid model

In recent years, research into extrasolar planetary systems has developed rapidly, and the constant influx of new data poses new challenges. The models of interacting and precessing Gauss rings provide a new interpretation of complex problems in perturbation theory and simplify calculations of the Lagrange perturbation function method. Among exoplanets, the class of hot Jupiters with large masses, orbits close to the central star, and relatively short periods of node precession is of particular interest. To solve these problems, the use of the R-toroid model is promising.

9.1 Some limitations on the application of the R-toroid model

It should be emphasized that the R-toroid model is intended for studying the secular evolution of outer orbits whose semimajor axes *exceed* a certain critical (minimum) value $a_{\min}$. For a known period of nodal precession of the disturbing body T_Ω the value $a_{\min}$ is calculated using the formula [27]

$$a_{\min} \approx \left(\frac{\kappa}{2\pi}T_\Omega\right)^{3/2}, \quad \kappa^2 = G(M+m)\,. \quad (9.1)$$

As an example, we will calculate $a_{\min}$ for the giant planets Jupiter and Saturn using formula (9.1). To do this, we need to know two periods: the period of the planet's motion around the Sun (it is well known $T_{\mathrm{orb}} \approx 11.862$ years) and the period of precession of the node of Jupiter's orbit $T_{J\Omega}$. According to [30], in a linear approximation, the corresponding period of nodal precession will be approximately equal to $T_{J\Omega} \approx 20370.84$ years. This is the characteristic time of the creation of the R-toroid for Jupiter, since on smaller time scales the figure of the R-toroid for Jupiter will not be complete. The angle of inclination of Jupiter's orbit to the ecliptic is currently small and equal to $i \approx 1^\circ.30327$. The width of the R-ring for Jupiter is $2ea \approx 0.50$ a.u. It follows that the secular influence of Jupiter's R-toroid can be considered only on those celestial bodies whose orbital semimajor axes satisfy the inequality $a \geqslant 747$ a.u. Therefore, for Jupiter $a_{\min} \approx 747$ a.u. Similar calculations for Saturn give $a_{\min} \approx 582$ a.u. Thus, R-toroid models for Jupiter and Saturn allow us to calculate secular effects not only in the motion of the hypothetical Planet 9 (with the parameters $a \approx 400-800$ a.u. adopted for it), but also in the motion of sednoids and some extreme trans-Neptunian objects (eTNOs).

We also present calculations $a_{\min}$ for some exoplanets.

PTFO 8-8695b

According to [32], the exoplanet PTFO 8-8695b (hot Jupiter) moves along a strongly inclined orbit around the central star. For this exoplanet $a = 0.0084$ a.u. and $T_{\mathrm{orb}} \approx 10.76$ h, therefore, PTFO 8-8695b is one of the exoplanets closest to the star. The critical value of the semimajor axis of the orbit $a_{\min}$ for it is only $a_{\min} \approx 0.2 \pm 0.7$ a.u. Thus, the R-toroid model for the planet PTFO 8-8695b allows us to describe the evolution of the orbits of bodies that are very close to the central star. It is noteworthy that the second planet in this system, PTFO 8-8695c, is very far from the central star $a = 662$ a.u. and obviously falls into the zone of gravitational influence of this R-toroid.

The exoplanet Kepler-413b

Consider the example of the Kepler-413b *circumbinary* planet. According to [31], it orbits with the period $T_{\mathrm{orb}} \approx 66.262$ d around a close pair of stars of classes K and M with masses $M_1 = 0.820 \pm 0.015 M_{\mathrm{e}}$ and $M_2 = 0.542 \pm 0.008 M_e$. The stars revolve around the center of mass in just 10.11615 ± 0.00001 d in almost circular orbits ($e = 0.037 \pm 0.002$). The radius and mass of the exoplanet are equal $R \approx 0.388 R_J$, $M \approx 0.2110 M_J$. According to these characteristics, this planet is close to hot Saturns. The parameters of the planet's orbit are equal $e = 0.118$, $q \approx 0.3553$ a.u., $i \approx 30^\circ$ and the period of nodal precession is $T_\Omega \approx 11$ yrs [31]. Accordingly, for this planet $T_\Omega/T_{\mathrm{orb}} \approx 60.83$ using these data, it is possible to calculate the critical value of the semimajor axis of the orbit, which turns out to be equal $a_{\min} \approx 5.48$ a.u. Thus, for the Kepler-413 system, the R-toroid model allows us to describe the evolution of test orbits located at moderate (several astronomical units) distances from the central star.

9.2 The two-planet problem (star + two planets)

The two-planet problem (star + two planets) is relevant for extrasolar systems. In the article [27], the ratios of nodal and apsidal precession periods for orbits were found

$$\frac{T_{1\Omega}}{T_{1\omega}} = \frac{m_1 + 2\kappa m_2}{m_1 + \kappa m_2}\,, \quad \frac{T_{2\Omega}}{T_{2\omega}} = \frac{2m_1 + \kappa m_2}{m_1 + \kappa m_2}\,, \quad (9.2)$$

(m_1 and m_2 are the masses of the planets). For verification, we note that applying formulas (9.2) to the 'Sun–Jupiter–Saturn' system gives $T_{j\Omega}/T_{j\omega} \approx 1.181$ something close to an accurate calculation $T_{j\Omega}/T_{j\omega} \approx 1.219$.

9.3 The ratio of nodal and apsidal precession periods

The ratio of the periods of nodal and apsidal precession of the orbit in the R-toroid field is [27]

$$\frac{T'_\Omega}{T'_\omega} = \left|\frac{\dot\omega}{\dot\Omega}\right| = \frac{5\cos^2 i' - 1}{2\cos i'} \approx 2\left(1 - \frac{3}{4}\, i'^2 + O(i'^6)\right). \quad (9.3)$$

It follows from (9.3) that the ratio of the periods of the nodal and apsidal precessions of the Gauss ring located in the gravitational field of the R-toroid weakly depends on the inclination of the ring and turns out to be slightly less than 2

$$\frac{T'_\Omega}{T'_\omega} \leqslant 2\,. \quad (9.4)$$

If perturbations from the central body are considered only, in particular $i = 0$ equation (9.3) gives $T_\Omega / T_\omega = 2$. This result is confirmed by numerical modeling of the dynamics of the exoplanet KOI 120.01 [31].

9.4 Secular evolution of exoplanetary systems. The three R-toroid method

To study the evolution of the orbits of circumbinary exoplanets, an extended method was developed in [29] using a system of three R-toroids; here, for each of the three bodies, its own R-toroid is created, describing a binary star and an exoplanet. Two tasks are considered. In the first one, the goal is to investigate the precession of test orbits in the force field of three R-toroids. The second problem uses the Gauss ring method to study the secular evolution of the orbits of stars and exoplanets in the circumbinary system itself.

In the first task, the apsidal and nodal precession of the trial orbit are investigated in the gravitational field of three R-toroids. To estimate the precession periods for the circumbinary planet Kepler-413b, it is necessary to consider the total contribution from three R-toroids: two R-toroids corresponding to the stars and one R-toroid for the planet. The necessary equations from (8.9) for each of the R-toroids are written as:

$$\begin{aligned} \left(\frac{\mathrm{d}\Omega}{\mathrm{d}t}\right)_R &= \dot\Omega_R^0 \left(\frac{1\ \text{a.u.}}{a}\right)^{7/2} \frac{\cos i}{(1-e^2)^2}\,, \\ \left(\frac{\mathrm{d}\omega}{\mathrm{d}t}\right)_R &= \dot\omega_R^0 \left(\frac{1\ \text{a.u.}}{a}\right)^{7/2} \frac{5\cos^2 i - 1}{4(1-e^2)^2}\,, \end{aligned} \quad (9.5)$$

where $R = \{1, 2, p\}$ is an index denoting a specific R-toroid ($R = 1, 2$ refers to a double star, $R = p$ refers to a planet). The frequency coefficients in (9.5) are equal

$$\dot\Omega_R^0 = \frac{3}{2}\, C_{20}^R\, \frac{m_R}{\bar M_R} \sqrt{\frac{G\bar M_R}{a_R^3}}\,, \quad \dot\omega_R^0 = -2\Omega_R^0\,, \quad (9.6)$$

$$\bar M_1 = \frac{M_2^3}{(M_1 + M_2)^2}\,, \quad \bar M_2 = \frac{M_1^3}{(M_1 + M_2)^2}\,, \quad (9.7)$$

and coefficients of zonal harmonics of R-toroids are

$$\begin{aligned} C_{20}^R &= -\frac{1}{2}\left(1 + \frac{3}{2}\, e_R^2\right) \frac{3\cos^2 i_R - 1}{2}\,, \\ C_{40}^R &= \frac{3}{8}\left(1 + 5e_R^2 + \frac{15}{8}\, e_R^4\right) \frac{35\cos^4 i_R - 30\cos^2 i_R + 3}{8}\,. \end{aligned} \quad (9.8)$$

As a result, we have expressions for the frequencies and periods of the trial planet

$$\begin{aligned} &\dot\Omega_{12p}^0 = \dot\Omega_1^0 + \dot\Omega_2^0 + \dot\Omega_p^0\,, \quad \dot\omega_{12p}^0 = -2\dot\Omega_{12p}^0\,, \\ &T_\Omega^{12p} = \frac{2\pi}{\left|(\mathrm{d}\Omega/\mathrm{d}t)_{12p}^0\right|}\,, \quad (T_\omega^{12p})_0 = \frac{1}{2}\, T_\Omega^{12p}\,. \end{aligned} \quad (9.9)$$

For the Kepler-413 system at $a = a_{\text{cr}}$, we have an estimate of the apsidal precession period $T_\omega^{12p} = (102 \pm 1)10^3$ yrs, and for the precession period of the longitude of the ascending node $T_\Omega^{12p} = (203 \pm 3) \times 10^3$ yrs.

The investigation of the secular evolution of orbits for a large selection of circumbinary exoplanets (on the basis of data from observations from [33]) according to the above method of three R-toroids was carried out in the article [29]. For each system from the sample, we: (a) created a superposition of three R-toroids, (b) estimated the angular moments of the star pair and the planet relative to the Laplace plane, (c) found the coefficients of the second and fourth zonal harmonics, and (d) derived and solved equations for the frequencies of both types of precession on the test orbits. In the gravitational field of an R-toroid, the ratio of the periods of apsidal and nodal precession on a Gaussian ring with zero slope is (-2).

10. Conclusion

The article provides an overview of four new analytical methods in modern dynamic astronomy: the method of Gaussian rings (and systems of such rings), the method of orbital orientation vectors, as well as methods based on two-dimensional (R-disks) and three-dimensional (R-toroids) calculations of models based on precessing Gaussian rings.

The method of finding the potential of the Gauss ring in analytical form is presented. To study the secular evolution of orbits, instead of osculating Keplerian elements, a method of new vector variables describing the shape and orientation of orbits was developed. These are the Laplace vector **L** the Hamilton vector **H** and the vector of the orbital angular momentum of the body **l**. If in the usual two-body problem these are vector integrals of motion, then in the problem with perturbations, instead of integrals of motion, we have functions of time. Taking into account these new variables, instead of the classical Lagrange equations, evolutionary equations for the three indicated orbital orientation vectors were obtained in the linear approximation. This new approach is used to study the secular evolution of exoplanets with arbitrary orbit orientation relative to the observation plane. The method has been tested on the exosystem HD 206893.

The actual problem of stabilizing the shape (confinement) of rings around small bodies of the Solar system is considered. These rings differ from planetary-type rings: they are narrow, typically located beyond the Roche limit of the central body, and lack shepherd satellites. It is also interesting that the motion of particles in the rings of small bodies is often in 3:1 spin-orbit resonance with the rotation of the central body. Therefore, the description of the secular evolution of rings and the development of mechanisms for preserving their shape is an urgent problem. To solve the retention problem, we examined the self-gravity mechanism of the rings. For this purpose, a model of two interacting Gauss rings has been developed.

An important part of this work is also the creation of two new models based on Gauss precessing rings — the R-ring and the R-toroid. Their construction method involves double and, respectively, triple averaging of the particle's motion over 'fast' variables. The structure of these new models and their spatial potential are considered in detail. Applications of these methods include studying the problem of precession of interacting stellar disks in the central parsec of the Galaxy and the secular evolution of orbits in two-planet and circumbinary exoplanetary systems. To study the secular evolution of exoplanet systems, a special method of three R-toroids was developed. Methods known from the literature for studying circumbinary systems turned out to be special cases of the approach developed here; our method of R-toroids additionally takes into account the eccentricities and inclinations of the orbits of bodies to the Laplace plane, as well as gravitational perturbation from the third body (planet).

References

1. Todhunter I *Istoriya Matematicheskikh Teorii Prityazheniya i Figury Zemli ot N'yutona do Laplasa* (Moscow: URSS, 2002); Translated from English: *A History of the Mathematical Theories of Attraction and the Figure of the Earth from the Time of Newton to that of Laplace* (London: Macmillan and Co., 1873)
2. Subbotin M F *Vvedenie v Teoreticheskuyu Astronomiyu* (Introduction to Theoretical Astronomy) (Moscow: Nauka, 1968)
3. Duboshin G N *Nebesnaya Mekhanika. Osnovnye Zadachi i Metody* (Celestial Mechanics. Fundamental Problems and Methods) (Moscow: Nauka, 1975)
4. Emelyanov N *Dinamika Estestvennykh Sputnikov Planet na Osnove Nablyudenii* (Fryazino: Vek 2, 2019); Translated into English: *The Dynamics of Natural Satellites of the Planets* (Amsterdam: Elsevier, 2020)
5. Kondratyev B P *Astron. Rep.* **67** 742 (2023); *Astron. Zh.* **100** 630 (2023)
6. Morbidelli A *Sovremennaya Nebesnaya Mekhanika. Aspekty Dinamiki Solnechnoi Sistemy* (Moscow–Izhevsk: Inst. Komp'yut. Issled., 2014); Translated from English: *Modern Celestial Mechanics* (London: Taylor and Francis, 2002)
7. Goldstein H, Poole C, Safko J *Klassicheskaya Mekhanika* (Moscow–Izhevsk: RKhD, 2012); Translated from English: *Classical Mechanics* 3rd ed. (San Francisco, CA: Addison Wesley, 2002)
8. Roseveare N T *Perigelii Merkuriya ot Lever'e do Einsteina* (Moscow: Mir, 1985); Translated from English: *Mercury's Perihelion from Le Verrier to Einstein* (Oxford: Clarendon Press, 1982)
9. NASA Exoplanet Archive. California Institute of Technology, https://exoplanetarchive.ipac.caltech.edu
10. Kondratyev B P, Kornoukhov V S, Kireeva E N *Moscow Univ. Phys. Bull.* **80** 349 (2025); *Vestn. Mosk. Univ. Ser. 3. Fiz. Astron.* **80** 2520802 (2025)
11. Hinkley S et al. (GRAVITY Collab.) *Astron. Astrophys.* **671** L5 (2023)
12. Kondratyev B P, Kornoukhov V S *Moscow Univ. Phys. Bull.* **80** (Suppl. 1) S34 (2025)
13. Mastroianni R, Efthymiopoulos Ch, in *Multi-Scale* (*Time and Mass*) *Dynamics of Space Objects, 18–22 October, 2021, Romania* (Proc. of the Intern. Astronomical Union, No. 364, Eds A Celletti et al.) (Cambridge: Cambridge Univ. Press, 2022) p. 191, DOI:10.1017/S1743921321001368
14. Kondratyev B P *Teoriya Potentsiala. Novye Metody i Zadachi s Resheniyami* (Theory of Potential. New Methods and Problems with Solutions) (Moscow: Mir, 2007)
15. Kondratyev B P *Solar Syst. Res.* **46** 352 (2012); *Astron. Vestn. Issled. Solnechnoi Sistemy* **46** 380 (2012)
16. Kondratyev B P *Solar Syst. Res.* **48** 366 (2014); *Astron. Vestn. Issled. Solnechnoi Sistemy* **48** 396 (2014)
17. Kondratyev B P, Kornoukhov V S *Astron. Rep.* **64** 434 (2020); *Astron. Zh.* **97** 408 (2020)
18. Gorkavyi N N, Fridman A M *Fizika Planetnykh Kolets. Nebesnaya Mekhanika Sploshnoi Sredy* (Moscow: Nauka, 1994); Translated into English: Fridman A M, Gorkavyi N N *Physics of Planetary Rings. Celestial Mechanics of Continuous Media* (Berlin: Springer-Verlag, 1999)
19. Braga-Ribas F et al. *Nature* **508** 72 (2014)
20. Ortiz J L et al. *Nature* **550** 219 (2017)
21. Kondratyev B P, Kornoukhov V S *Mon. Not. R. Astron. Soc.* **478** 3159 (2018)
22. Pereira C L et al. *Astron. Astrophys.* **673** L4 (2023)
23. Kondratyev B P, Kornoukhov V S *Astron. Rep.* **68** 688 (2024); *Astron. Zh.* **101** 660 (2024)
24. Kondratyev B P, Trubitsina N G, Mukhametshina E S, in *Order and Chaos in Stellar and Planetary Systems, Proc. of the Conf., 17–24 August, 2003, St. Petersburg, Russia* (ASP Conf. Proc., Vol. 316, Eds G G Byrd et al.) (San Francisco, CA: Astronomical Society of the Pacific, 2004) p. 326
25. Kondratyev B P *Mon. Not. R. Astron. Soc.* **442** 1755 (2014)
26. Kondratyev B P, Klyuchinsky K A *Moscow Univ. Phys. Bull.* **79** 627 (2024); *Vestn. Mosk. Univ. Ser. 3 Fiz. Astron.* **79** 2450881 (2024)
27. Kondratyev B P, Kornoukhov V S *Astron. Rep.* **65** 412 (2021); *Astron. Zh.* **98** 407 (2021)
28. Kondratyev B P, Kornoukhov V S *Astron. Rep.* **65** 588 (2021); *Astron. Zh.* **98** 571 (2021)
29. Kondratyev B P, Kornoukhov V S *Astron. Rep.* **66** 1063 (2022); *Astron. Zh.* **99** 1029 (2022)
30. Simon J L et al. *Astron. Astrophys.* **282** 663 (1994)
31. Welsh W F et al. *Astrophys. J.* **809** 26 (2015)
32. Raetz St et al. *Mon. Not. R. Astron. Soc.* **460** 2834 (2016)
33. Kostov V B et al. *Astrophys. J.* **784** 14 (2014)